THE JOURNAL OF BIOLOGICAL CHEMISTRY VOL. 291, NO. 26, pp. 13546–13559, June 24, 2016

Molecular Basis of Transient Neonatal Zinc Deficiency

*NOVEL ZnT2 MUTATIONS DISRUPTING ZINC BINDING AND PERMEATION**

Received for publication, April 14, 2016 Published, JBC Papers in Press, May 2, 2016, DOI 10.1074/jbc.M116.732693

Yarden Golan[‡1], Naoya Itsumura[§1], Fabian Glaser[¶], Bluma Berman[‡], Taiho Kambe[§2], and Yehuda G. Assaraf[‡3]

From the [‡]Department of Biology, Fred Wyszkowski Cancer Research Laboratory and the [¶]Bioinformatics Knowledge Unit, The Lorry I. Lokey Interdisciplinary Center for Life Sciences and Engineering, Technion, Haifa 32000, Israel and the [§]Division of Integrated Life Science, Graduate School of Biostudies, Kyoto University, Kitashirakawa-Oiwake-cho, Sakyo-ku, Kyoto 606-8502, Japan

A gradually increasing number of transient neonatal zinc deficiency (TNZD) cases was recently reported, all of which were associated with inactivating *ZnT2* mutations. Here we characterized the impact of three novel heterozygous ZnT2 mutations G280R, T312M, and E355Q, which cause TNZD in exclusively breastfed infants of Japanese mothers. We used the bimolecular fluorescence complementation (BiFC) assay to provide direct visual evidence for the *in situ* dimerization of these ZnT2 mutants, and to explore their subcellular localization. Moreover, using three complementary functional assays, zinc accumulation using BiFC-Zinquin and Zinpyr-1 fluorescence as well as zinc toxicity assay, we determined the impact of these ZnT2 mutations on vesicular zinc accumulation. Although all three mutants formed homodimers with the wild type (WT) ZnT2 and retained substantial vesicular localization, as well as vesicular zinc accumulation, they had no dominant-negative effect over the WT ZnT2. Furthermore, using advanced bioinformatics, structural modeling, and site-directed mutagenesis we found that these mutations localized at key residues, which play an important physiological role in zinc coordination (G280R and E355Q) and zinc permeation (T312M). Collectively, our findings establish that some heterozygous loss of function ZnT2 mutations disrupt zinc binding and zinc permeation, thereby suggesting a haploinsufficiency state for the unaffected WT *ZnT2* allele in TNZD pathogenesis. These results highlight the burning need for the development of a suitable genetic screen for the early diagnosis of TNZD to prevent morbidity.

In the past 50 years, the key role of zinc in human health was established (1). Zinc is crucial for central physiological processes including DNA and protein synthesis, enzyme activity, intracellular signaling, immune function, fertility, as well as growth and development (1–3). Zinc homeostasis is primarily regulated by two zinc transporter families as well as by zinc-binding proteins. The *SLC39A* gene family encodes for ZIP1–14 transporters, which are responsible for zinc uptake into the cytosol from the extracellular fluid or from intracellular vesicles (4). In contrast, the *SLC30A* gene family encodes for the transporters ZnT1–10, which are responsible for zinc secretion from the cytosol to intracellular organelles or through the plasma membrane outside the cells (2, 4).

The recent position of the Academy of Nutrition and Dietetics (5) is that breastfeeding in the first 6 months of life can provide adequate micronutrients and macronutrients for optimal growth and development. This statement is correct for the vast majority of infants around the world. However, recent reports indicate that some exclusively breastfed infants suffer from severe zinc deficiency due to lack of zinc in the breast milk they consume (6–11). These cases were referred to as transient neonatal zinc deficiency (TNZD),[4] as the symptoms can be treated with zinc supplementation to the diet of the infant (12, 13). In contrast to TNZD, which appears only in exclusively breastfed infants, and will not emerge after weaning, acrodermatitis enteropathica (OMIM number 201100), an autosomal recessive disease (12, 14), also presents after weaning, as a result of loss of function mutations in the *SLC39A4* gene (*ZIP4*). These inactivating mutations impair intestinal zinc absorption via the ZIP4 transporter, thereby leading to severe zinc deficiency after weaning. This zinc deficiency can lead to death in the absence of adequate zinc supplementation (13). To date, eight loss of function mutations were identified in the *SLC30A2* (*ZnT2*) gene, which cause TNZD (6–11) (OMIM number 608118) and at least 20 cases of infants with TNZD were reported in the past eight years in Japan (11). Current data suggest that 36% of 54 women who were tested had an exon variation in the *SLC30A2* gene, and exhibit inadequate or excess zinc levels in their breast milk (15).

The *SLC30A2* gene encodes for the zinc transporter ZnT2, which is responsible for zinc accumulation in intracellular vesicles, in lactating epithelial mammary gland cells. Through exocytosis, these zinc-loaded vesicles secrete zinc into breast milk (13). The molecular mechanisms that were found to be causative of TNZD included aggresomal accumulation (6), dominant-negative effect (8, 16, 17), frameshift mutation, which causes premature translation termination (9), disruption of homodimer formation (7), and enhanced degradation of ZnT2 (7). Excluding one case of compound *ZnT2* mutations (7), all TNZD cases reported to date were found in mothers that were heterozygous for mutations in the *SLC30A2* gene.

* The authors declare that they have no conflicts of interest with the contents of this article.

[1] Both authors contributed equally to this work.

[2] To whom correspondence may be addressed. Tel.: 81-75-753-6273; Fax: 81-75-753-6274; E-mail: kambe1@kais.kyoto-u.ac.jp.

[3] To whom correspondence may be addressed. Tel.: 972-4-8294211; Fax: 972-4-8225153; E-mail: assaraf@tx.technion.ac.il.

[4] The abbreviations used are: TNZD, transient neonatal zinc deficiency; BiFC, bimolecular fluorescence complementation; PTEN, phosphatase and tensin homolog; TM, transmembrane; ER, endoplasmic reticulum.

TABLE 1
Primers used to introduce site-directed mutations into the human ZnT2 cDNA at amino acid positions Gly-280, Thr-312, and Glu-355

Experiment	Name	Forward sequence (5′ to 3′)	Reverse sequence (5′ to 3′)
Zinc toxicity assay	ZnT2 G280R	GTGTTGATGGAAAGGACCCCCAAGGGC	GCCCTTGGGGGTCCTTTCCATCAACAC
	ZnT2 G280A	GTGTTGATGGAAGCTACCCCCAAGGGC	GCCCTTGGGGGTAGCTTCCATCAACAC
	ZnT2 G280T	GTGTTGATGGAAACGACCCCCAAGGGC	GCCCTTGGGGGTCGTTTCCATCAACAC
	ZnT2 G280L	GTGTTGATGGAACTGACCCCCAAGGGC	GCCCTTGGGGGTCAGTTCCATCAACAC
	ZnT2 G280Q	GTGTTGATGGAACAGACCCCCAAGGGC	GCCCTTGGGGGTCTGTTCCATCAACAC
	ZnT2 G280K	GTGTTGATGGAAAAGACCCCCAAGGGC	GCCCTTGGGGGTCTTTTCCATCAACAC
	ZnT2 T312M	ATCTGGGCACTGATGGTGGCCCAGCCT	AGGCTGGGCCACCATCAGTGCCCAGAT
	ZnT2 T312A	ATCTGGGCACTGGCGGTGGCCCAGCCT	AGGCTGGGCCACCGCCAGTGCCCAGAT
	ZnT2 T312S	TGGGCACTGAGCGTGGCCCAG	CTGGGCCACGCTCAGTGCCCA
	ZnT2 T312C	ATCTGGGCACTGTGCGTGGCCCAGCCT	AGGCTGGGCCACGCACAGTGCCCAGAT
	ZnT2 T312E	TGGGCACTGGAGGTGGCCCAG	CTGGGCCACCTCCAGTGCCCA
	ZnT2 T312D	TGGGCACTGGACGTGGCCCAG	CTGGGCCACGTCCAGTGCCCA
	ZnT2 E355Q	GTGACCATCCAGATCCAGGACTACTCGGAG	CTCCGAGTAGTCCTGGATCTGGATGGTCAC
	ZnT2 E355A	ACCATCCAGATCGCTGACTACTCGGAG	CTCCGAGTAGTCAGCGATCTGGATGGT
	ZnT2 E355D	ACCATCCAGATCGACGACTACTCGGAG	CTCCGAGTAGTCGTCGATCTGGATGGT
BiFC assay	ZnT2 G280R	GTGATCCTGGTGTTGATGGAAAGGACCCCCAAGGGCGTTGAC	GTCAACGCCCTTGGGGGTCCTTTCCATCAACACCAGGATCAC
	ZnT2 T312M	GCACTGATGGTGGCCCAGCCTGTTCTG	CAGAACAGGCTGGGCCACCATCAGTGC
	ZnT2 E355Q	ATCCAGATCCAGGACTACTCGGAGGAC	GTCCTCCGAGTAGTCCTGGATCTGGAT

We recently applied the bimolecular fluorescence complementation (BiFC) assay to provide the first evidence for the homo- and heterodimerization of various members of the ZnT family (16, 17). Here we employed this BiFC technique along with an advanced bioinformatics analysis, using three-dimensional modeling, which is based upon the crystal structure of the bacterial YiiP, a ZnT homologue from *Escherichia coli*, to functionally characterize three novel mutations in the *ZnT2* (*SLC30A2*) gene, which were recently shown to cause TNZD in Japanese infants (11). These novel *ZnT2* mutations provide new insight into the structure and function of the C terminus of ZnT2 transporter with emphasis on the disruption of zinc binding and zinc permeation capacity. These novel mutations markedly expand our knowledge regarding structural ZnT2 determinants of zinc binding and transport.

Materials and Methods

Chemicals and Reagents—The DNA dye Hoechst 33342 was purchased from Sigma. The viable fluorescent zinc probe Zinquin ethyl ester was purchased from Biotium (Hayward, CA), whereas zinc sulfate was obtained from Merck. The second zinc probe, Zinpyr-1 ester was purchased from Santa Cruz Biotechnology (Santa Cruz, CA).

Expression Vector Construction—Expression plasmids used to express C terminally HA- or FLAG-tagged ZnT2 were constructed by inserting the cDNA into the pA-puro or pA-Neo vectors. For zinc toxicity assay the introduction of a mutation into *ZnT2* cDNA was carried out by the two-step PCR method, and amplified cDNAs were sequenced in both directions. The primers for the introduction of *ZnT2* mutations are listed in Table 1. *ZnT2* BiFC constructs were generated as previously described (17). The mutations were introduced into the *ZnT2* expression plasmids using Pfu Turbo DNA polymerase (QuikChange kit, Stratagene, La Jolla, CA) and the primers listed in Table 1. Plasmid containing the ER marker β-subunit of the signal recognition receptor tagged with CFP (SRβ-CFP) was kindly provided by Hirschberg Koret (Tel-Aviv University, Israel).

Stable Expression of ZnT2 Protein in DT40 $ZnT1^{-/-}MT^{-/-}ZnT4^{-/-}$ Cells—For electroporation, chicken B lymphocyte-derived DT40 cells deficient in *ZnT1*, *metallothionein* (*MT*), and *ZnT4* genes ($ZnT1^{-/-}MT^{-/-}ZnT4^{-/-}$ cells) (2×10^7) were suspended in 0.5 ml of PBS containing 25 μg of linearized DNA. DNA was electroporated into the cells by Gene Pulser Xcell (Bio-Rad) under conditions of 550 V and 25 μF with a 0.4-cm gap electroporation cuvette. After electroporation, cells were transferred into 30 ml of growth medium and incubated for 24 h. Cells were then resuspended in 60 ml of growth medium containing 0.5 μg/ml of puromycin (Sigma) or 2 mg/ml of G418 (Sigma) and divided into three 96-well plates. After 10 days, drug-resistant clones were transferred to 24-well plates in 1 ml of selection medium and cultured for 2 days. Expression of ZnT2 was confirmed by Western blot analysis. More than three independent clones per transfection were picked.

Western Blotting Analysis—The blotted PVDF membrane (Immobilon-P, Millipore Corp., Bedford, MA) was blocked with a solution of 5% skimmed milk and 0.1% Tween 20 in PBS prior to incubation with anti-DDDDK tag (1:4,000, MBL, Nagoya, Japan, PM020), anti-HA HA-11 (1:4,000, Covance, Emeryville, CA, MMS-101P), anti-ZnT2 (7) (1:4,000 dilution), or anti-β-tubulin (1:10,000, Sigma, T7816) antibodies in blocking solution. Horseradish peroxidase-conjugated anti-mouse (GE Healthcare, NA931) or anti-rabbit (GE Healthcare, NA934) secondary antibodies, were added at a 1:4,000 dilution for detection. The fluoro-image was obtained using LAS1000 plus (Fujifilm, Tokyo, Japan).

Transient Transfections—MCF-7 breast cancer cells were grown and transiently transfected as previously described (17). Cells were seeded in 12-well plates (10^5 cells/well; Nunc A/S, Roskilde, Denmark) for flow cytometry studies. For fluorescence microscopy cells were seeded (2×10^5 cells/well) in 24-well glass bottom plates (In Vitro Scientific, Sunnyvale, CA) with 1 ml of growth medium containing the transfection reagents and plasmids. Cells were transiently transfected (0.5 μg of ER marker plasmid DNA + 0.5 μg of BiFC constructs/well, total 1 μg of DNA/well) using linear polyethylenimine (M_r = 25,000) transfection reagent (Polysciences, PA) at a ratio of 3:1 μg of polyethylenimine:DNA, and were incubated for up to 24 h before imaging.

Evaluation of Zinc Transport Activity of ZnT2 Mutants Based on a Viability of Zinc-sensitive DT40 $ZnT1^{-/-}MT^{-/-}ZnT4^{-/-}$ Cells against High Levels of Extracellular Zinc—DT40 $ZnT1^{-/-}MT^{-/-}ZnT4^{-/-}$ cells were cultured in RPMI 1640 (Nacalai Tesque, Kyoto, Japan) supplemented with 10% (v/v)

heat-inactivated fetal calf serum (FCS; Multiser, Trace Scientific, Melbourne, Australia), 1% (v/v) chicken serum (Invitrogen), and 50 μM 2-mercaptoethanol (Sigma) at 39.5 °C as previously described (7, 18). *ZnT1*$^{-/-}$*MT*$^{-/-}$*ZnT4*$^{-/-}$ cells failed to grow in the presence of ≥60 μM $ZnSO_4$ (7, 18). To evaluate cell viability in the presence of increasing extracellular zinc concentrations, cells were cultured in the presence of 50–100 μM $ZnSO_4$ for 72 h. Viable cell numbers were determined by trypan blue exclusion, and relative cell viability was determined as previously described (7). Relative values presented are evaluations of the averages of three independent experiments. Each evaluation was performed at least three times.

Fluorescence Microscopy—Twenty-four h after transfection, the growth medium was removed and monolayer cells were washed with PBS and incubated in PBS containing 1 mM $MgCl_2$, 1 mM $CaCl_2$, and 10 mM D-glucose, pH 7.4. Hoechst 33342 (2 μg/ml) was used for nuclear DNA staining. Live cells were imaged using an inverted confocal microscope (Zeiss LSM 710) at a magnification of ×63 under immersion oil.

Flow Cytometry—For the BiFC-Zinquin assay, transiently transfected MCF-7 cells were analyzed by flow cytometry for both YFP fluorescence as well as fluorescence of the viable zinc probe, Zinquin, as previously described (16). In addition, *ZnT1*$^{-/-}$*MT*$^{-/-}$*ZnT4*$^{-/-}$ cells stably expressing each ZnT2 mutant were grown in the presence or absence of 30 μM $ZnSO_4$ for 48 h then treated with 5 μM Zinpyr-1 ester for 30 min before being analyzed by flow cytometer as previously described (11).

BiFC Terminology—YN and YC represent the N- and C-terminal halves of YFP, respectively. Transfection with the construct-YC-YN implies that plasmids containing both the construct-YN and construct-YC were co-transfected into cells.

Structural Modeling of Human ZnT2—ZnT2 monomer model was aligned to the 3h90 template (PDB code 3h90, chains A and C) using the HHpred method (19), and its three-dimensional structure modeled by MODELLER software (20) using the HHpred interface. To obtain the ZnT2 dimer, we performed structural alignment of two identical modeled monomers of ZnT2 with two crystal structures of YiiP monomers, which form one of the two unit cell dimers. Then, mutations were introduced with Swapaa in Chimera UCSF (21), and visualized with its interface. The three-dimensional structural model of the ZnT2 dimer was obtained by superimposing two monomers of the ZnT2 model into the 3h90 dimer, using the MatchMaker tool on Chimera UCSF (21, 22). Because the mutations are on the cytoplasmic domain, structural alignment was performed using only this region for maximal accuracy. For that purpose, we used only 82 residues from the C-terminal cytoplasmic domain of both molecules, corresponding to amino acids 359–278 in ZnT2 and 287–206 in YiiP, because the three mutations in this study were mapped to the cytoplasmic region and local comparison of corresponding residues is more accurate with this structural alignment. This procedure yielded a very good root mean square deviation of 0.455 (compared with a root mean square deviation 0.697 Å for the full model). Subsequent analyses of the localization and possible impact of mutations were undertaken with the dimer model of the human ZnT2 obtained. Stability calculations of the ZnT2 monomer upon introduction of individual mutations were carried out with FoldX (23) and DUET (24) servers.

FoldX is a computational method that provides quantitative estimation of the importance of the interactions contributing to the stability of proteins. It provides an estimation of the free energy (in kcal/mol). FoldX predictions are relevant when the energy difference can be calculated between two well defined structures, such as between the WT and a mutant. The difference in the calculated free energies ($\Delta\Delta G$) between the final state (the mutant) and the reference state (the WT protein) correlates well with the experimentally observed change in stability (23).

DUET is an integrated computational approach for the assessment of the impact of missense mutations on protein stability. DUET combines mCSM and SDM methods in a consensus prediction, by consolidating the results of the separate methods in an optimized predictor using support vector machines trained with Sequential Minimal Optimization (24). Molecular graphics and analyses were performed with the UCSF Chimera package (21).

MatchMaker extension (22) of Chimera UCSF is a structural alignment tool that works by first constructing a pairwise sequence alignment and then used to superimpose the structures. The fit can be improved iteratively by pruning residue pairs far apart in space.

AreaSAS Attribute (on Chimera UCSF)—The solvent-accessible surface area was available when a molecular surface was computed. Swapaa command in UCSF Chimera replaces amino acid side chains using information from a rotamer library. Rotamers can be chosen automatically based on the lowest clash score, mostly H-bonds, best fit to an electron density map, and/or highest probability according to the library, or interactively from a rotamer list.

HHpred server (19) for the protein remote homologue detection and three-dimensional structure prediction is a sequence database searching and structure prediction algorithm that is much more sensitive than BLAST in identifying remote homologues. HHpred can produce pairwise query-template sequence alignments, merged query-template multiple alignments (*e.g.* for transitive searches), as well as three-dimensional structural models calculated by the MODELLER software from HHpred alignments with very low sequence identity.

Statistical Analysis—Results are presented as mean ± S.D. Statistical comparisons were performed using Student's *t* test (Prism GraphPad, Berkeley, CA), and a significant difference was demonstrated when p was < 0.05. Results from at least three independent experiments are shown.

Results

The TNZD Mutations G280R, T312M, and E355Q Retain ZnT2 Homodimerization—We first assessed the ability of the ZnT2 mutants to form homodimers using the BiFC assay and flow cytometric analysis. In this respect, we determined two parameters. (*a*) The percentage of cells displaying YFP fluorescence and (*b*) the median cellular YFP fluorescence. These parameters reflected the ability of ZnT2 monomers (ZnT2-YC and ZnT2-YN) to form homodimers. Consequently, the two non-fluorescent halves of the YFP protein refolded and yielded

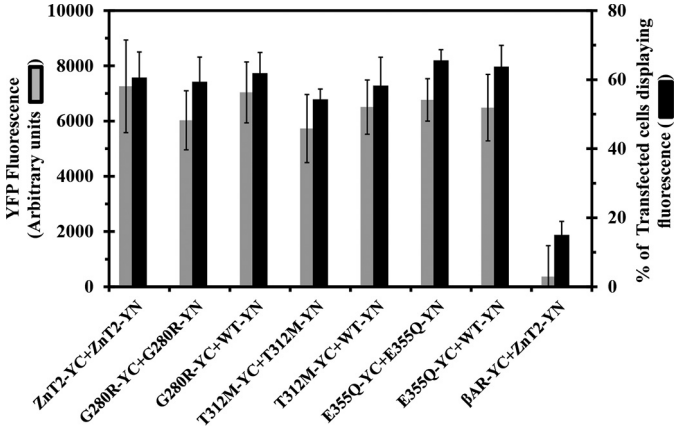

FIGURE 1. **ZnT2 mutants form homodimers based on BiFC analysis.** MCF-7 cells were transiently co-transfected with YC- and YN-tagged ZnT2 plasmid pairs or with β2AR-YN as detailed below in the *x* axis. The percentage of transfected cells displaying YFP fluorescence (*black bars*) and the median YFP fluorescence (*gray bar*) were determined using flow cytometry and represent the fraction of ZnT-YC-YN positive cells. The negative controls consisted of co-transfection with ZnT2-YC and β2AR-YN. All *p* values ($p < 0.05$) revealed statistically significant differences when compared with the negative control of ZnT2-YC + β2AR-YN. All *p* values ($p < 0.05$) of the different mutants did not display any statistically significant differences when compared with WT-ZnT2-YC-YN. *Error bars* represent S.D.

a strong YFP fluorescence signal. The ZnT2 mutants G280R, T312M, and E355Q neither significantly diminished the percentage of cells displaying YFP fluorescence nor the median YFP fluorescence compared with the WT-ZnT2 (Fig. 1). These results indicate that none of these ZnT2 mutations interfered with the homodimerization capacity. Moreover, this YFP fluorescence was preserved when cells were co-transfected with YC-YN pairs of a given mutant plasmid (*G280R-YC-YN, T312M-YC-YN,* or *E355Q-YC-YN*) as well as upon co-transfection of a single mutant along with WT-*ZnT2-YN* (*G280R-YC+ZnT2-YN, T312M-YC+ZnT2-YN,* or *E355Q-YC+ZnT2-YN*). These results are consistent with a previous co-immunoprecipitation analysis, indicating that these ZnT2 mutants interact with the WT-ZnT2, hence corroborating the preservation of homodimerization of these ZnT2 mutants (11).

Certain ZnT2 Mutations Alter the Subcellular Localization of ZnT2 Homodimers—MCF-7 cells were transiently co-transfected with WT or mutant *ZnT2* BiFC constructs, and were analyzed using confocal microscopy to explore the impact of the mutations on the subcellular localization of ZnT2 homodimers (as summarized in Table 2). WT-ZnT2 homodimers were found to localize in intracellular vesicles (Fig. 2, *a–c*), which are responsible for zinc accumulation as previously shown (16). In contrast, the G87R-ZnT2 dominant-negative TNZD mutant was retained in the ER as evident from the co-localization of G87R-ZnT2 with SRβ-CFP, an established ER marker (Fig. 2, *d–f*). Similarly, most of the fluorescent G280R-YC-YN dimers were localized at the ER network (Fig. 2, *j–l*) and failed to reach their physiologic secretory vesicles destination. Homodimers of G280R-YC+WT-ZnT2-YN were found to localize at the ER in a large fraction of transfectant cells (Fig. 2, *g–i*). However, some vesicular localization was also observed indicating that some of these homodimers reached their physiologic vesicular destination, and could potentially contribute to vesicular zinc accumulation. These findings suggest that upon homodimerization, the mutant G280R alters the subcellular localization of the WT ZnT2; however, in contrast to the G87R mutant (8, 17), G280R did not fully abolish the ability of the WT-ZnT2 to reach its intracellular vesicular destination. In contrast, approximately half of the cells transfected with the mutant T312M-YC-YN showed vesicular localization, whereas the remaining fraction of cells displayed ER retention (Fig. 2, *p–r*). These results suggest that mutant-mutant T312M ZnT2 homodimers significantly retained some of their native vesicular localization. Furthermore, T312M-YC+WT-ZnT2-YN dimers were localized predominantly in intracellular vesicles (Fig. 2, *m–o*), suggesting that the T312M mutant has little deleterious effect on the localization of the WT-ZnT2 upon dimerization. Finally, E355Q-YC-YN dimers displayed a predominant ER retention (Fig. 2, *v–x*), whereas E355Q-YC+WT-ZnT2-YN homodimers exhibited a vesicular localization in a large fraction of transfectant cells (Fig. 2, *s–u*), when compared with the mutant-mutant pairs. These results suggest that the E355Q mutation has a deleterious effect on the native subcellular localization of WT-ZnT2 upon homodimerization.

G280R, T312M, and E355Q Mutants Disrupt Zinc Transport but Do Not Exert a Dominant-negative Effect Over the WT ZnT2—To assess the functionality of the mutant ZnT2 dimers, flow cytometry dot plot analysis was undertaken to compare YFP fluorescence *versus* the fluorescence of Zinquin, a viable cellular zinc probe (Fig. 3). The background autofluorescence dot plot of non-transfected cells defined the quadrant position. The upper quadrants (left and right) represent cells displaying YFP fluorescence above the background level, hence being indicative of intact formation of ZnT2 homodimers. The upper right quadrant reflects cells displaying YFP and Zinquin fluorescence levels above the background. To calculate Zinquin accumulation (shown in Fig. 4), we divided the percentage of cells displaying YFP and Zinquin fluorescence (upper right quadrant) by the percentage of cells displaying YFP fluorescence (upper quadrants). When WT-*ZnT2-YC-YN* constructs were co-transfected, a large fraction (>40%) of cells were in the upper right quadrant, and only a small fraction (~20%) was at the upper left quadrant (Fig. 3*b*). These results demonstrate that from a total of 60% of cells displaying YFP fluorescence, the majority accumulated Zinquin. Hence, this indicated the functionality of WT-ZnT2 homodimers in zinc accumulation (Fig. 3*b*). Importantly, the dot plots clearly demonstrate the functional differences between WT-ZnT2 and the different ZnT2 mutants; in contrast to the WT-*ZnT2-YC-YN* transfection, when both YC and YN constructs of *ZnT2* were mutated (Fig. 3, *c*, *e*, and *g*), most of the cells were located at the upper left quadrant, indicating a very low Zinquin accumulation, as a result of the loss of vesicular zinc transport (Fig. 3, *c*, *e*, and *g*). These results were similar to transfection with the empty *YFP* vector (Fig. 3*i*), which was used as a negative control for lack of zinc transport activity. However, when WT-*ZnT2-YN* was co-transfected together with mutant-*ZnT2-YC* constructs, there was a shift toward the upper right quadrant (Fig. 3, *d*, *f*, and *h*), indicating the rescue of the zinc transport function by the WT-mutant pairs, when compared with the mutant-mutant ZnT2 dimers that were inactive in zinc transport (Fig. 3, *c, e*, and *g*). Similar results were obtained when WT-*ZnT2-YC* was trans-

TABLE 2
Summary of the multi-factorial effects of the various TNZD ZnT2 mutants

	Method/details	G280R	T312M	E355Q
mRNA level (11)	**Location at the gene**	Exon 6–7	Exon 7	Exon 8
	Nucleotide change	Guanine 838 to adenine	Cytosine 935 to thymine	Guanine 1063 to cytosine
	Impact on splicing	Reduced splicing efficiency by 75% relative to WT	No deleterious effect expceted	No deleterious effect expceted
Location in ZnT2 protein	**Predicted location based on the three-dimensional model**	Loop between the last transmembrane (TM) helix and a cytoplasmic domain	Loop between β-sheets of a cytoplasmic domain, being in close proximity to TM helices	Solvent-exposed residue in the C terminus
Protein levels and stability	**ZnT2 mutant degradation (11)**[a]	80% Enhanced degradation compared with WT	40% Enhanced degradation compared with WT	60% Enhanced degradation compared with WT
	Protein levels upon stable co-transfection with WT-ZnT2 (Fig. 5)[b]	Low expression compared with the WT	High expression compared with the WT	Slightly reduced expression compared with the WT
	Mutant protein levels under stable transfection (Fig. 8)[c]	Slightly reduced expression compared with the WT	Slightly reduced expression compared with the WT	Very low expression compared with the WT
	BiFC assay (Fig. 1)	Same YFP intensity levels as the WT	Same YFP intensity levels as the WT	Same YFP intensity levels as the WT
	Calculated thermodynamic destabilization (Table III)	Very unstable	Stable	Unstable
Subcellular localization of ZnT2	**Mutant-mutant pairs-BiFC assay (Fig. 2)**	Nearly all cells displayed ER localization	Half of the cells showed ER localization and half vesicular localization	Most of the cells showed ER localization
	Mutant-WT pairs-BiFC assay (Fig. 2)	Some vesicular localization was observed in most cells	Most cells preserved vesicular localization	Half of the cells showed ER localization and half vesicular localization
Dimerization	**Immunoprecipitation analysis (11)**	Forms homodimers with the WT protein	Forms homodimers with the WT protein	Form Homodimers with the WT protein
	BiFC assay (Fig. 1)	Forms homodimers at the same level of the WT protein	Forms homodimers at the same level of the WT protein	Form homodimers at the same level of the WT protein
Function	**Zinc toxicity assay**	Mutant non-functional; restored the ability to protect cells upon co-expression with WT-ZnT2	Mutant non-functional; restored the ability to protect cells upon co-expression with WT-ZnT2	Mutant non-funct ional; restored the ability to protect cells upon co-expression with WT-ZnT2
	Zinpyr-1 accumulation	Mutant non-functional	Mutant non-functional	Mutant non-functional
	Zinquin accumulation	Mutant non-functional. Yet, did not completely abolish the ability of the WT-ZnT2 protein to accumulate zinc	Mutant non-functional. Yet, did not completely abolish the ability of the WT-ZnT2 protein to accumulate zinc	Mutant non-functional. Yet, did not completely abolish the ability of the WT-ZnT2 protein to accumulate zinc
Zinc coordination	**Based on the three-dimensional model**	Close to zinc coordination site B in YiiP	Surrounded by conserved polar amino acids that are probably important for zinc transport	Direct coordination of zinc, on the equivalent site C of Y iiP
Zinc levels in breast milk (time after birth)	**Normal levels: 80 ± 30 μg/dl at 4–6 months (11)**	10 μg/dl (4 months)	<10 μg/dl (6 months)	21 μg/dl (4 months)
Age of infant upon TNZD onset (11)		3 months	5 months	1.5 months

[a] Determined by Western blotting analysis after cycloheximide treatment of the different mutants that were stably transfected into DT40 $ZnT1^{-/-}$ $MT^{-/-}ZnT4^{-/-}$ cells.
[b] Determined by Western blot analysis of the different mutants that were stably co-transfected with WT-ZnT2 into DT40 $ZnT1^{-/-}$ $MT^{-/-}$ $ZnT4^{-/-}$ cells.
[c] Determined by Western blot analysis of the different mutants that were stably transfected into DT40 $ZnT1^{-/-}$ $MT^{-/-}$ $ZnT4^{-/-}$ cells.

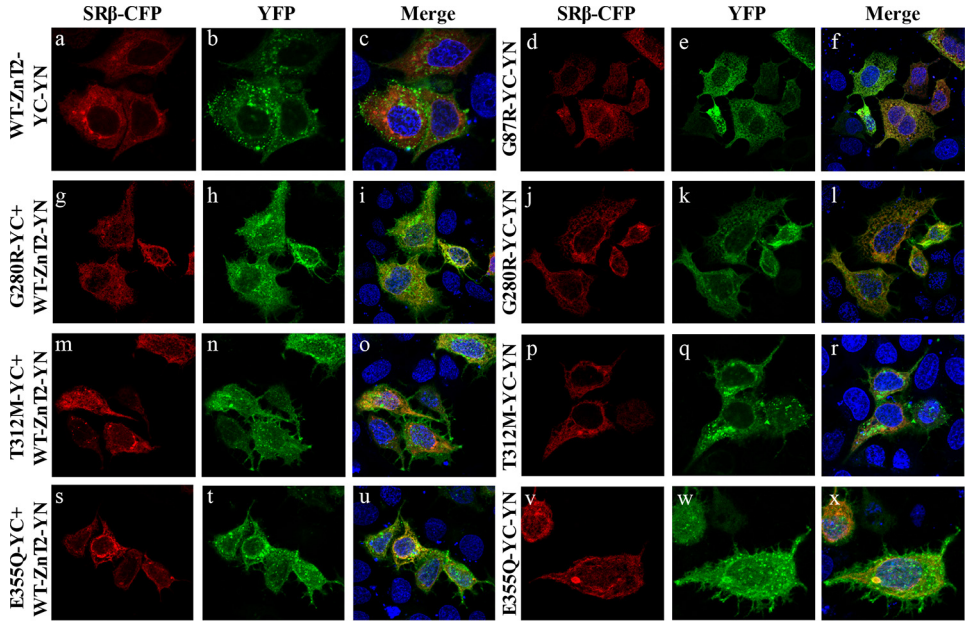

FIGURE 2. **Subcellular localization of WT ZnT2 and mutant homodimers.** MCF-7 cells were transiently co-transfected with the constructs described at the *left side* of the triplet panels. In addition, cells were co-transfected with the construct of the ER marker, the *β* subunit of signal recognition receptor tagged with CFP (SR*β*-CFP), *left panels*. The *green* YFP fluorescence signal (YC-YN fluorescence) at the *middle panels* indicates dimer formation. Hoechst 33342 (*blue* fluorescence) was used to stain nuclei. Live MCF-7 cells were examined using confocal (LSM 710) fluorescence microscopy. A magnification of ×63 under immersion oil was used.

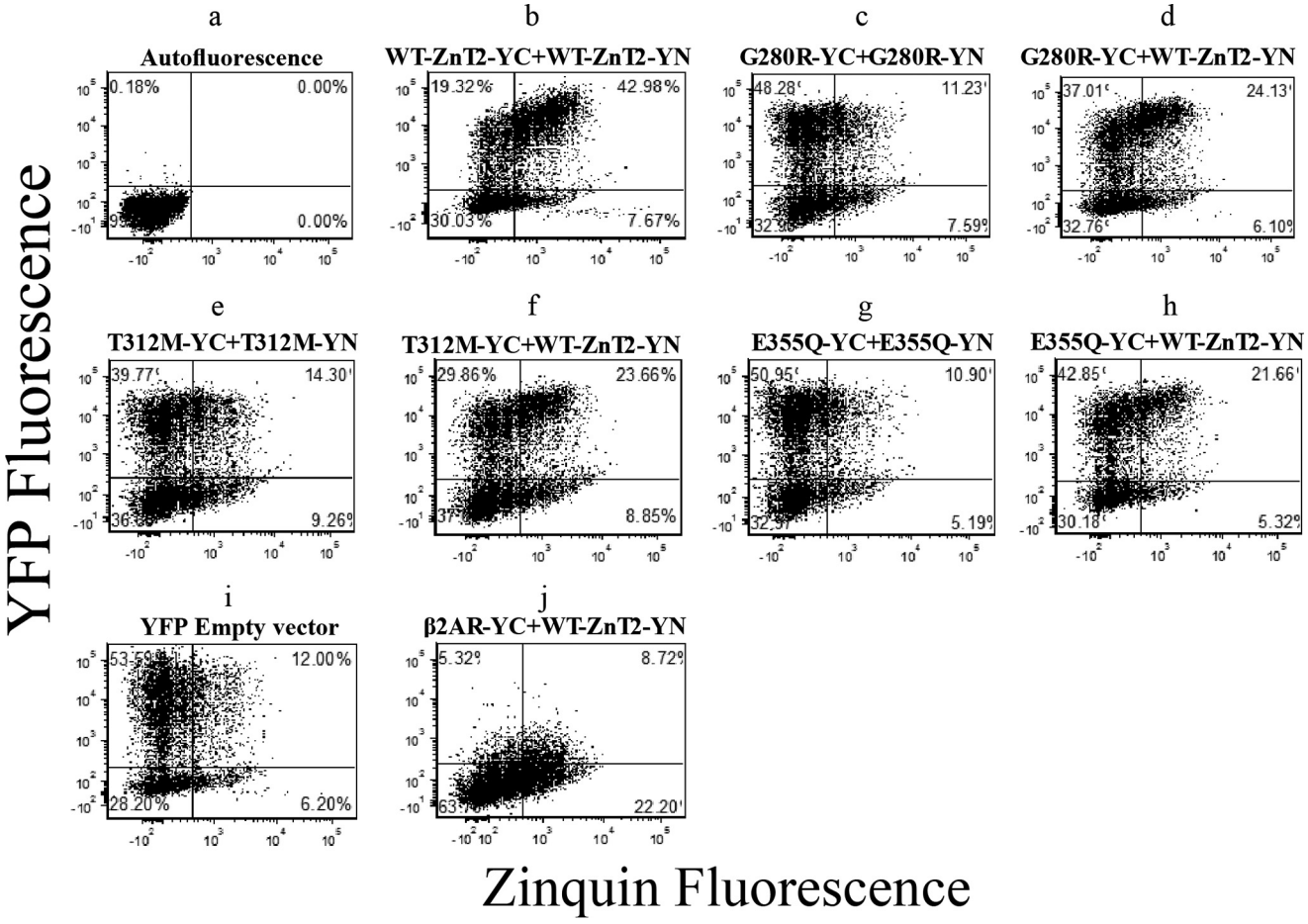

FIGURE 3. **Flow cytometry dot-plot analysis was undertaken to assess the functionality of the ZnT2 mutants.** Shown are flow cytometry dot-plots from one representative experiment. MCF-7 cells were transiently co-transfected with the constructs described above the dot-plots. The *y*-axis represents the YFP fluorescence, whereas the *x*-axis denotes Zinquin fluorescence levels. Each *dot* represents a single cell. Quadrants were determined using the autofluorescence dot-plot. *Upper* quadrants represent all cells displaying an YFP fluorescence level that was above the autofluorescence signal (transfected cells). *Right* quadrants represent all cells displaying Zinquin fluorescence. *Upper-right* quadrants represent cells exhibiting both YFP signal and Zinquin staining.

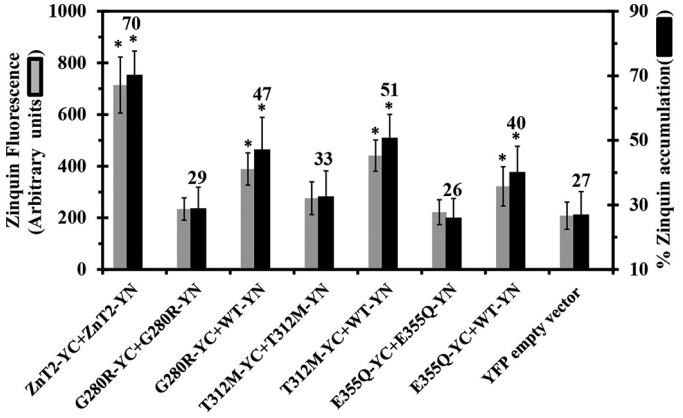

FIGURE 4. **Zinquin accumulation assay reveals the disruption of zinc transport function in various ZnT2 mutants associated with TNZD.** MCF-7 cells co-transfected with the constructs depicted along the *x* axis were examined for Zinquin fluorescence levels (*gray bars*) as well as the percentage of transfected cells displaying Zinquin fluorescence (*dark bars*). The percentage of Zinquin accumulation was calculated by dividing the fraction of YFP fluorescent cells (YC-YN) displaying Zinquin fluorescence by the total fraction of cells displaying YFP fluorescence (YC-YN). *Asterisks* indicate that the values obtained were significantly different ($p < 0.05$) when compared with the YFP empty vector. *Error bars* represent S.D.

fected together with mutant-*ZnT2-YN* constructs (data not shown). This dot plot analysis highlights the differences between different ZnT2 mutants and the WT transporter in Zinquin accumulation and the major deleterious effect these mutations have on zinc transport.

We next determined Zinquin fluorescence intensity and cellular accumulation levels in the different ZnT2 variants using flow cytometry (Fig. 4). We found that Zinquin accumulation levels (Fig. 4, *black bars*) obtained with the mutant-mutant pairs (*i.e.* G280R-YC-YN, T312M-YC-YN, and E355Q-YC-YN) were not significantly different from the Zinquin accumulation levels of the empty vector transfection. These results highlight the major deleterious effect that these TNZD mutations have on the zinc transport capacity of ZnT2. In contrast, when WT-ZnT2-YN was co-transfected with one of the mutants, G280R-YC, T312-YC, or E355Q-YC, the presence of the WT-ZnT2 transporter significantly improved Zinquin accumulation when compared with the empty vector; albeit, they did not attain the Zinquin accumulation levels of the WT-ZnT2 pairs (Fig. 4, left-most column, *black bars*). Furthermore, in all co-transfections with mutant and WT ZnT2, Zinquin fluorescence levels were significantly higher when compared with the empty vector (Fig. 4, *gray bars*). These results indicate that these ZnT2 mutants did not exert a dominant-negative effect over the WT-ZnT2, as Zinquin accumulation levels and fluorescence levels were significantly higher when the mutant was expressed together with the WT-ZnT2.

To further explore the impact of each of the three mutants on the function of the WT-ZnT2 upon co-expression, hence mimicking the heterozygous mutation found in the mothers of TNZD patients, we used a cell-based zinc toxicity assay in DT40 cells that lack *ZnT1*, *metallothionein*, and *ZnT4* ($ZnT1^{-/-}MT^{-/-}ZnT4^{-/-}$) as previously described (7, 18). We compared the viability of cells stably expressing WT-ZnT2 and/or mutant ZnT2 upon a cytotoxic challenge of increasing zinc concentrations. Moreover, the ability of the different

TABLE 3

Cell-based zinc toxicity in DT40 cells stably transfected with various site-directed ZnT2 TNZD mutants

The viability of cells exposed to the indicated concentrations of $ZnSO_4$ for 72 h was determined by determining the number of viable cells using Trypan blue exclusion. The results of single transfectant cells (G87R, G280R, T312M, or E355Q) were recently published (7). Relative values presented are evaluations of the average values of three independent experiments.

	$ZnSO_4$ (μM)					
Expressed ZnT2	50	60	70	80	90	100
DT40 $ZnT1^{-/-}MT^{-/-}ZnT4^{-/-}$ cells						
Untransfected	+++[a]	−	−	−	−	−
WT-HA	+++	+++	+++	+++	+++	++
G87R-HA	+++	−	−	−	−	−
G280R-HA	+++	−	−	−	−	−
T312M-HA	+++	−	−	−	−	−
E355Q-HA	+++	−	−	−	−	−
DT40 $ZnT1^{-/-}MT^{-/-}ZnT4^{-/-}$ cells						
WT-HA + WT-FLAG	+++	+++	+++	+++	+++	++
WT-FLAG + G87R-HA	+++	+++	++	+	−	−
WT-HA + G280R-FLAG	+++	+++	+++	+++	++	+
WT-HA + T312M-FLAG	+++	+++	+++	+++	++	+
WT-HA + E355Q-FLAG	+++	+++	+++	+++	+++	++

[a] The symbols represent: +++: growing to confluence; ++, +: decreased growth (20–50% or up to 20% relative to +++); −, no growth.

mutants to protect cells against zinc toxicity was compared with the G87R-ZnT2 mutant, which we have previously shown to exert a dominant-negative effect over the WT-ZnT2 (8, 17). When different tagged WT-ZnT2 was expressed alone, cells survived up to a concentration of 100 μM $ZnSO_4$, hence recapitulating the key protective role of ZnT2 via vesicular zinc compartmentalization (Table 3). In contrast, single ectopic gene expression of each of the ZnT2 mutants, including G87R, G280R, T312M, and E355Q, did not confer upon cells any protective effect against $ZnSO_4$ and all cells died when exposed to >60 μM $ZnSO_4$ as previously shown (Table 3). Co-expression of WT-ZnT2 along with G87R-ZnT2 slightly improved the ability of cells to tolerate high zinc levels, up to 80 μM $ZnSO_4$ (Table 3). The expression levels of G87R-ZnT2 were relatively low when compared with the WT-ZnT2 protein, although the total ZnT2 expression levels in these cells were higher than that in the cells expressing the WT-ZnT2 alone (Fig. 5). These results suggest that the dominant-negative effect of G87R over the WT protein is even more significant when considering its low expression level. Surprisingly, in contrast to the G87R-ZnT2, co-expression of the WT-ZnT2 along with single mutants, including G280R-ZnT2, T312M-ZnT2 and E355Q-ZnT2, substantially improved the ability of cells to tolerate high zinc levels up to 100 μM $ZnSO_4$. Zinc tolerance activity in cells co-expressing WT-ZnT2 and the E355Q mutant was the same as in cells expressing the WT-ZnT2. Co-expression of WT-ZnT2 together with G280R or T312M appeared to provide zinc torelance activity, which was slightly lower than WT-ZnT2 expression (Table 3). These three stably expressing transfectants displayed a better zinc tolerance capacity when compared with the co-expression of the WT-ZnT2 and G87R. The expression levels of G280R-ZnT2 and E355Q-ZnT2 were further evaluated using Western blotting analysis and were found to be relatively lower than WT-ZnT2 levels in cells co-expressing both mutants (Fig. 5). This may suggest that in these cells, in contrast to the dominant-negative effect we observed with the G87R mutant, more active homodimers of WT-ZnT2 were formed, which presumably better protected the cells from zinc

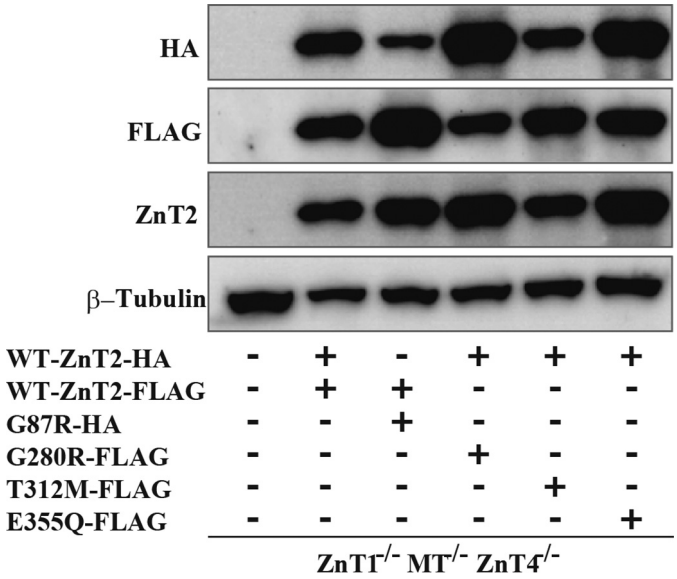

FIGURE 5. **Co-expression levels of WT and mutant ZnT2 in DT40 *ZnT1*$^{-/-}$ *MT*$^{-/-}$*ZnT4*$^{-/-}$ cells.** Confirmation of stable co-expression of WT and mutant ZnT2 in DT40 *ZnT1*$^{-/-}$*MT*$^{-/-}$*ZnT4*$^{-/-}$ cells. Western blotting analysis was performed using antibodies against HA tag, FLAG tag, ZnT2, and β-tubulin. Total cellular protein aliquots (10 μg) were loaded onto each lane, and the same membrane was used for detection of ZnT2-HA, ZnT2-FLAG, and β-tubulin. β-Tubulin is shown as a loading control.

toxicity. These results (summarized in Table 2) lend further support to the Zinquin accumulation results and indicate that the G280R, T312M, and E355Q mutants did not exert a dominant-negative effect over the WT-ZnT2 as did the mutant G87R, although it was considered that they may exert a dominant-negative effect in a previous study (11).

Evaluation of the Impact of the Mutations on the Structure and Function of Human ZnT2—We undertook *in silico* mutation studies with three complementary approaches. (a) Using the ZnT2 dimer model and *in silico* introduction of the mutations using the Swapaa tool from UCSF Chimera (see "Materials and Methods"), we analyzed the energetic stability of the mutations when compared with the WT-ZnT2 using the DUET and FoldX methods. (*b*) Comparing the mutation positions and environment with the corresponding YiiP residues. (*c*) Analyzing the impact on zinc binding, of the ZnT2 mutations, which are in close proximity to zinc ions in the YiiP crystal structure. The three mutations including G280R, T312M, and E355Q (11) were found to localize at sites critical for the zinc transport function of ZnT2 as shown in our three-dimensional model (Fig. 6) and as discussed below.

The G280R Mutation—Gly-280 is located in a loop between the last transmembrane (TM) helix and a cytoplasmic domain

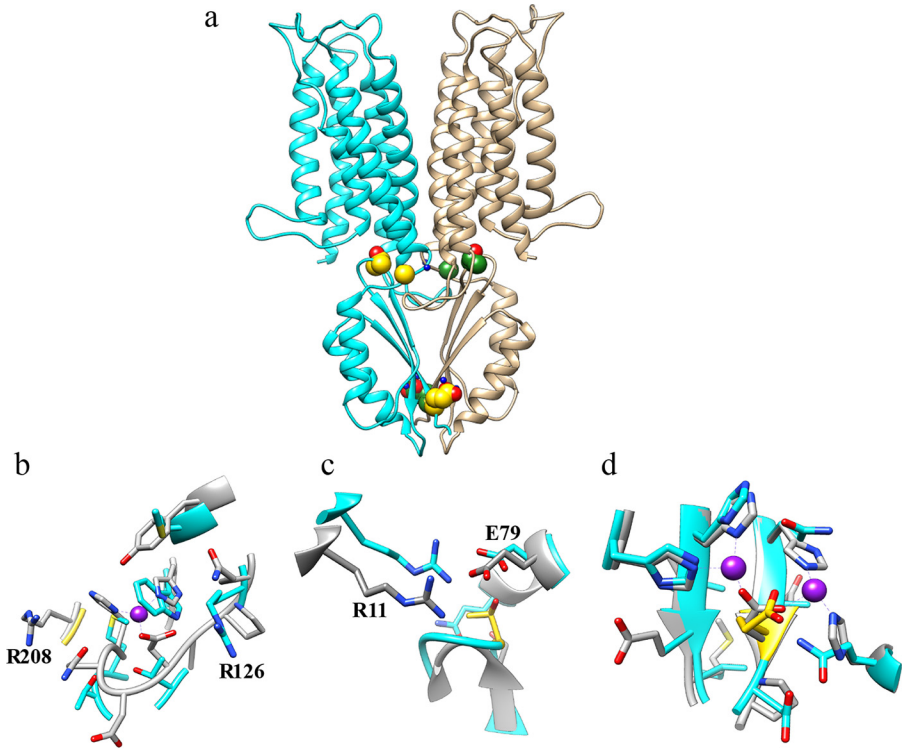

FIGURE 6. **Three-dimensional structural modeling of the human ZnT2.** The ZnT2 monomer model was aligned to the PDB code 3h90 template by the HHpred method as described under "Materials and Methods." (*a*) monomer ribbons are colored in *cyan* and *tan*, respectively, and the positions of the various ZnT2 mutations are shown in CPK (Corey-Pauling-Koltun) representation (available in Chimera), where carbon atoms are colored in *gold* and *green* for the two different monomers, respectively. Zinc ions from the YiiP model are shown (for approximate location only) in *blue* CPK balls. (*b*) the Microenvironment of Gly-280 in the human ZnT2 model; the carbon atoms of Gly-280 are colored in *gold*. (*c*) The environment of Thr-312 in the human ZnT2 model. (*d*) The environment of Glu-355 in the human ZnT2 model; the proximity to the two zinc atoms from the YiiP crystal structure and the two histidine residues (which are also present on YiiP), strongly suggests that Glu-355 is directly involved in zinc coordination. The mutation sites are colored in *gold*. Carbons of the ZnT2 model colored in *cyan* and carbons of the YiiP colored in *gray*. Oxygen atoms are colored in *red* and nitrogen atom in *blue*. Zinc atoms are colored in *violet*.

TABLE 4

Predicted thermodynamic destabilization of ZNT2 human monomer upon mutation expressed as the variation in Gibbs' free energy ($\Delta\Delta G$) in Kcal/mol

Positive values indicate stabilizing mutations while negative values denote destabilizing mutations (significant changes are estimated $> \pm 0.5$ kcal/mol).

Mutant	Duet server $\Delta\Delta G$	FoldX server $\Delta\Delta G$
G280R	−0.80	−1.72
T312M	−0.20	0.30
E355Q	−1.06	−0.59

TABLE 5

Zinc toxicity assay with site-directed mutations at positions Gly-280, Thr-312, and Glu-355

The viability of cells exposed to the indicated concentrations of $ZnSO_4$ for 72 h, was determined by counting the number of viable cells using Trypan blue exclusion. Relative values presented are the mean values of three independent experiments.

Expressed ZnT2	$ZnSO_4$ (μM) 50	60	70	80	90	100
DT40 *ZnT1*$^{-/-}$*MT*$^{-/-}$*ZnT4*$^{-/-}$ cells						
Untransfected	+++[a]	−	−	−	−	−
WT-HA	+++	+++	+++	+++	+++	++
DT40 *ZnT1*$^{-/-}$*MT*$^{-/-}$*ZnT4*$^{-/-}$ cells						
G280R-HA	+++	−	−	−	−	−
G280A-HA	+++	+++	+++	+++	+++	++
G280T-HA	+++	+++	++	+	−	−
G280L-HA	+++	−	−	−	−	−
G280Q-HA	+++	−	−	−	−	−
G280K-HA	+++	−	−	−	−	−
DT40 *ZnT1*$^{-/-}$*MT*$^{-/-}$*ZnT4*$^{-/-}$ cells						
T312M-HA	+++	−	−	−	−	−
T312A-HA	+++	−	−	−	−	−
T312S-HA	+++	+++	+++	+++	+++	++
T312C-HA	+++	+++	+++	++	+	−
T312D-HA	+++	−	−	−	−	−
T312E-HA	+++	−	−	−	−	−
DT40 *ZnT1*$^{-/-}$*MT*$^{-/-}$*ZnT4*$^{-/-}$ cells						
E355Q-HA	+++	−	−	−	−	−
E355A-HA	+++	−	−	−	−	−
E355D-HA	+++	+	−	−	−	−

[a] The symbols represent: +++, cells growing to confluence; ++, +, decreased cell growth (20–50 or up to 20% relative to +++); −, no growth.

in both the YiiP and ZnT2 structures. As evident from Fig. 6, *a* and *b*, and as revealed by surface accessibility calculated by Chimera (attribute areaSAS), residue Gly-280 is exposed to the solvent. The Gly-280 residue is located close to zinc coordination site B in YiiP (25). Although site B is not conserved in ZnT2, and therefore one cannot infer from our model that a zinc coordination site exists in ZnT2 near Gly-280. However, we note that the corresponding residue in the YiiP structure is an Arg (Arg-208), which interacts and stabilizes site B electrostatically (the distance of Arg-208 to zinc is 6.8 Å). Thus, interestingly, this mutation of glycine to arginine in ZnT2 is paradoxically disturbing the delicate balance of electrostatic properties in that region in ZnT2 that has evolved differently from YiiP, hence no longer allowing a charged residue in this position. However, the mutant arginine residue in ZnT2 (*i.e.* G280R) introduces an unnecessary positive charge, and a very large side chain whose size and bulk are expected to result in steric clashes with the second ZnT2 monomer. Additionally, we noticed that in ZnT2 there is a unique Arg-126 on the opposite side of the binding site (Gln-65 in YiiP) within almost the same distance of the zinc atom from the YiiP model as Arg-208 (Fig. 6*b*). This Arg-126 in ZnT2 may elicit the same stabilizing role of Arg-208 in YiiP. Therefore, we suggest the existence of a distinctly evolved zinc coordination site in ZnT2 formed by Met-132 and Trp-136 as well as Arg-126, instead of corresponding residues His-71, His-75, and Arg-208 in YiiP. Clearly, the G280R mutation in ZnT2 certainly introduces an additional unnecessary positive charge and presumably impairs proper electrostatic zinc coordination. Alternatively, if no direct zinc coordination site exists, the G280R mutation is expected to disrupt dimer formation and subcellular localization (also based on electrostatics and steric changes, and as evident from our BiFC assay, Fig. 2) or to reduce zinc transport turnover (*i.e.* additional positive charge will repel positive zinc ion in its out of the TM region en route out of the ER lumen). This is in fact the mutation that is predicted to exert the most profound energetic destabilization impact on the ZnT2 monomer (Table 4), which suggests a strong impact on protein stability, dimer formation, subcellular localization, and ultimately zinc transport.

The T312M Mutation—This mutation maps to a loop between β-sheets of a cytoplasmic domain of ZnT2, being in close proximity to TM helices. However, Thr-312 is completely buried and points toward the inner channel of the TM domain. The methionine residue is more hydrophobic and slightly larger than threonine. Notably, Thr-312 (Ser-239 in YiiP) forms a cluster with the surrounding residues Glu-140 (Glu-79 in YiiP), Arg-72 (Arg-11 in YiiP), and Gln-137 (Gly-76 in YiiP) in ZnT2 (Fig. 6*c*), which are polar amino acids and highly conserved as well as very tightly packed and hence are likely important for zinc transport. On the YiiP structure, the equivalent position to the cluster centered on Thr-312 in ZnT2 is very similar and identical in nearby residues Glu-140 (Glu-79 in YiiP) and Arg-72 (Arg-11 in YiiP), suggesting that they play a conserved functional role, probably in zinc transport. This is the mutation predicted to have the least impact on protein monomer stability (Table 4) and as revealed by the cycloheximide protein stability assay, which showed that the T312M ZnT2 is the most stable protein when compared with G280R and E355Q (11), suggesting a direct effect on the charge of the local structure or coordination of zinc along the zinc permeation pathway (Fig. 6, *a* and *c*).

The E355Q Mutation—Glu-355 is a completely solvent-exposed residue (as calculated by areaSAS, its exposed surface area in Chimera is very large) and presumably involved in direct coordination of zinc, on the equivalent site C of YiiP (25). Its conserved structural partner Asp-285 (and two conserved His residues) in YiiP is in close contact with one of the zinc ions (Fig. 6 d). Hence, its substitution to glutamine is expected to produce a pronounced deleterious impact on zinc coordination and consequently zinc transport. The E355Q mutation is also predicted to impact monomer stability but less than G280R (Table 4), because glutamate and glutamine residues are very similar, and therefore should not affect dimer formation (Fig. 6*a*); indeed, the BiFC assay confirmed that the E355Q mutation did not interfere with its homodimerization capacity (Fig. 1).

Mutational Analysis of the Gly-280, Thr-312, and Glu-355 Residues—To further corroborate the functional role of the Gly-280, Thr-312, and Glu-355 residues we performed mutational analysis using cell-based zinc toxicity assay in DT40 *ZnT1*$^{-/-}$*MT*$^{-/-}$*ZnT4*$^{-/-}$ cells (Table 5). In addition, we evaluated the zinc accumulation ability of these cells using the

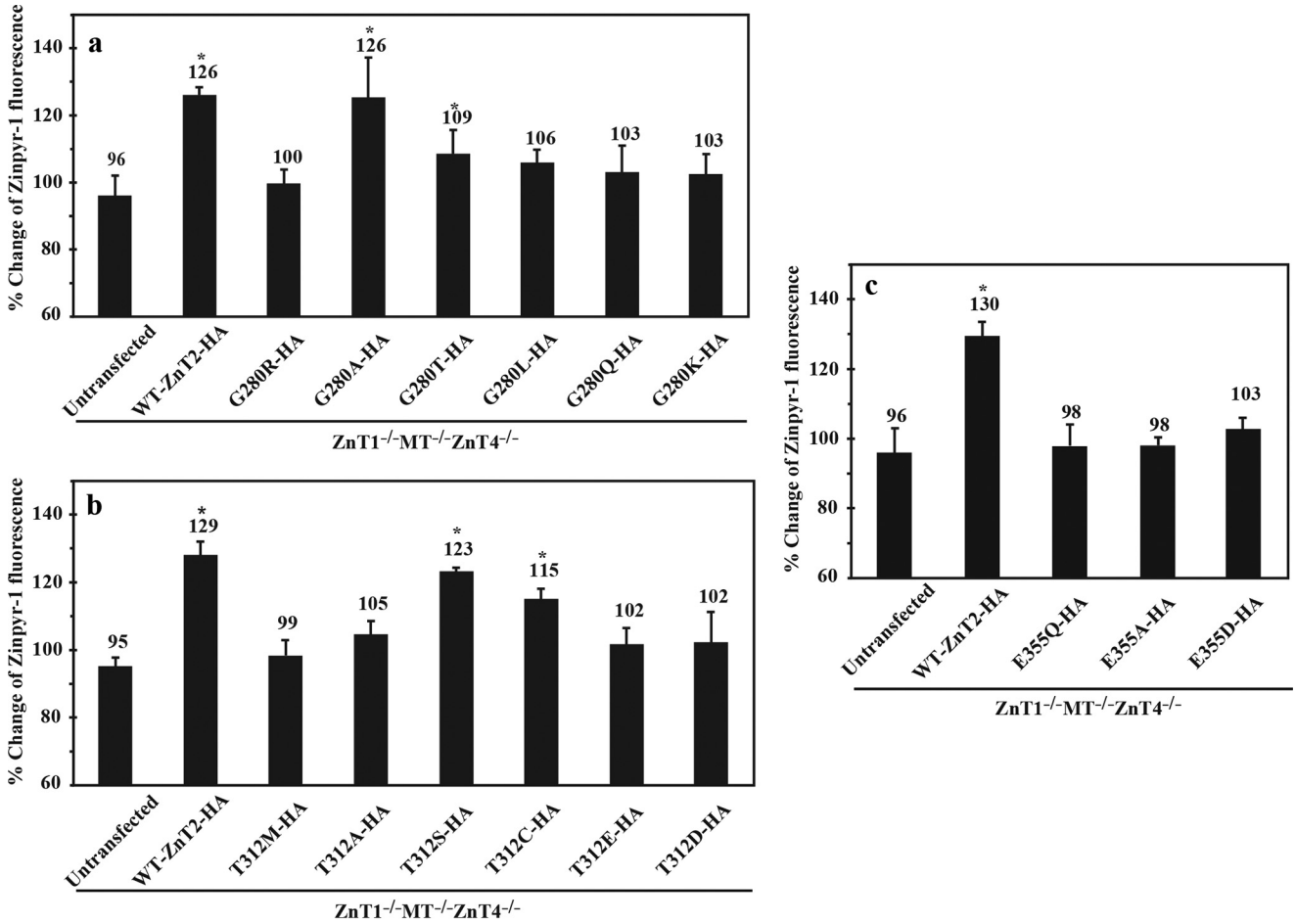

FIGURE 7. **Evaluation of the zinc transport activity of ZnT2 mutants of Gly-280, Thr-312, or Glu-E355 residues using a viable fluorescent zinc-selective probe, Zinpyr-1.** The percent changes of Zinpyr-1 fluorescence were calculated by dividing the fluorescence levels (raw value of medians) obtained in cells cultured in 30 μM $ZnSO_4$ by that under normal growth conditions. *Asterisks* denote a significant difference ($n = 3$, $p < 0.05$) in the percent, compared with the *ZnT1*$^{-/-}$*MT*$^{-/-}$*ZnT4*$^{-/-}$ cells stably expressing TNZD mutants (G280R, T312M, or E355Q). *Error bars* represent S.D.

selective zinc probe Zinpyr-1 and flow cytometry (Fig. 7). Expectedly, substitution of glycine 280 to alanine (G280A) fully preserved the ability of cells to protect themselves against zinc toxicity (Table 5) and accumulate Zinpyr-1 (Fig. 7*a*). This ability was partly preserved upon substitution of this glycine 280 to threonine mutation (G280T), as some cells survived up to a concentration of 80 μM $ZnSO_4$ (Table 5). In addition, these cells displayed slightly higher levels of Zinpyr-1 fluorescence compared with the G280R mutant (Fig. 7*a*). All other substitutions including G280L, G280Q, and G280K representing hydrophobic, polar, and cationic amino acid substitutions, respectively, failed to protect the cells from zinc toxicity and were similar to the G280R TNZD mutant (Table 5 and Fig. 7*a*). These results suggest that a small, non-polar, non-hydrophobic and non-charged amino acid is required in this position for proper function of ZnT2.

Next, we substituted the threonine residue at position 312 of ZnT2 as shown in Table 5 and Fig. 7*b*. Substitution of threonine 312 by alanine (T312A), glutamate (T312E), or aspartate (T312D) resulted in the loss of the ability of cells to protect themselves against zinc toxicity; cells failed to survive $ZnSO_4$ concentrations >60 μM, hence being similar to cells expressing the TNZD T312M mutation. In contrast, replacement of this residue with a nucleophilic amino acid such as serine (T312S) or cysteine (T312C) markedly restored cell survival under high zinc concentrations, with a slight advantage for the conservative serine substitution over cysteine. These results further support our findings that Thr-312 is presumably important for zinc chelation and coordination, which are essential prerequisites for zinc transport. Furthermore, we observed similar results in the Zinpyr-1 accumulation assay as substitution of the Thr-312 residue with the nucleophilic amino acids serine (T312S) or cysteine (T312C) significantly increased their ability to accumulate Zinpyr-1 compared with the T312M mutant, hence attaining the same Zinpyr-1 levels of the WT-ZnT2 (Fig. 7*b*).

Substitution of glutamate 355 to alanine (E355A), did not improve zinc transport ability when compared with the E355Q TNZD mutant, as *ZnT1*$^{-/-}$*MT*$^{-/-}$*ZnT4*$^{-/-}$ cells expressing E355Q or E355A were not able to tolerate $ZnSO_4$ concentrations >60 μM (Table 5). Furthermore, substitution of glutamate 355 to aspartate (E355D), which is the same amino acid that is present at the parallel residue (Asp-285) of zinc coordination in the bacterial YiiP, failed to rescue the zinc transport ability of ZnT2, and thus cells succumbed at concentrations >60 μM $ZnSO_4$. In addition, the ability of these mutant transporter expressing cells to accumulate Zinpyr-1 was similar to cells

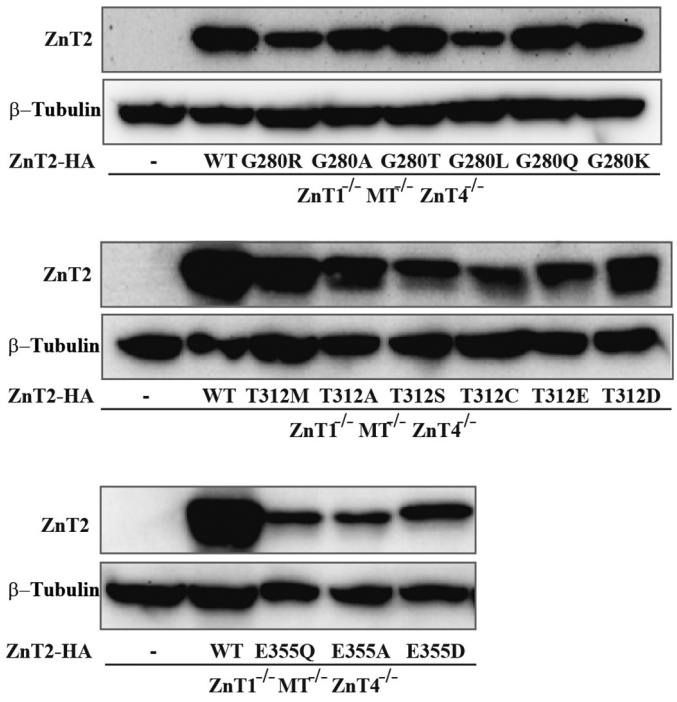

FIGURE 8. **Expression levels of the various Gly-280, Thr-312, and Glu-355 site-directed mutants of ZnT2 in DT40 *ZnT1*$^{-/-}$*MT*$^{-/-}$*ZnT4*$^{-/-}$ cells.** Confirmation of stable expression of the ZnT2-HA mutants in DT40 *ZnT1*$^{-/-}$*MT*$^{-/-}$ *ZnT4*$^{-/-}$ cells. Western blotting analysis was performed using anti-ZnT2 and β-tubulin antibodies. Aliquots (10 μg) of total cellular protein were loaded onto each lane, and the same membrane was used for detection of both ZnT2 and β-tubulin. β-Tubulin is shown to estimate the actual loading of the amount of proteins. − represents untransfected cells.

expressing the E355Q ZnT2 mutant (Fig. 7*c*). These results suggest that Glu-355 is crucial for zinc transport and compartmentalization, and emphasize that in contrast to YiiP, the aspartate residue at position 355 in ZnT2 is not sufficient for zinc coordination and cannot contribute to zinc transport function. Thus, the consistent results we obtained in the two different functional assays further strengthen the validity of these findings.

Different Expression Levels of the Various Gly-280, Thr-312, and Glu-355 Site-directed Mutants of ZnT2 in ZnT1$^{-/-}$*MT*$^{-/-}$ *ZnT4*$^{-/-}$ *Cells*—We determined the actual expression levels of these different mutations using Western blotting analysis to verify that the impaired function is not only due to low expression levels of the ZnT2 mutants (Fig. 8). We found that all mutant ZnT2 proteins were expressed at lower levels than the WT-ZnT2 protein (Fig. 8). However, these low expression levels were sufficient to support a markedly improved survival of cells expressing T312S or T312C proteins in a zinc toxicity assay (Table 5), thereby suggesting that the low expression levels are not the sole mechanism underlining the very low zinc compartmentalization ability of the other ZnT2 mutants as shown in Table 5 and Fig. 7.

Discussion

ZnT2 is a key mediator of zinc transport into vesicles in mammary gland epithelial cells (2, 26). It is the sole transporter, the loss of function of which was found to cause zinc-deficient breast milk and TNZD (6–11, 27). Here we studied the impact of three novel ZnT2 mutations recently identified in Japanese mothers of infants displaying TNZD (11), on the structure, stability, subcellular localization, and zinc transport function. These mutations, including G280R, T312M, and E355Q, mapped to the C terminus of ZnT2 (Fig. 6) in contrast to the G87R and W152R mutations that were found to be located in TM domains (7, 8), whereas H54R localized at the N terminus (6). Furthermore, these mutations mapped to ZnT2 residues that are apparently crucial for zinc binding and translocation, can shed light on the role of the C terminus of ZnT2 in protein stability and zinc transport. Specifically, the g838 to a838 (guanine 838 to adenine) mutation reduced splicing efficiency of intron 6 in the *ZnT2* transcript as shown previously (11). However, it is important to understand the impact of the G280R mutation as it was a heterozygous mutation, the remaining WT allele was not sufficient to support adequate zinc transport levels into the milk. We found that upon intact splicing, the G280R mutation altered the subcellular localization of ZnT2 and consequently impaired vesicular zinc transport as reflected in the loss of Zinquin and Zinpyr-1 accumulation. Furthermore, this G280R mutation, which mapped to the distal part of the zinc permeation pathway, could plausibly affect zinc coordination and/or transport, based on the introduction of a new positively charged Arg residue (Fig. 6), which is rather intriguing as it renders ZnT2 more similar to YiiP in this particular region. Despite that the close microenvironment of this Arg residue in YiiP is not conserved in ZnT2, one cannot rule out the possible existence of an alternative, nearby zinc coordination site on ZnT2, or a zinc permeation pathway leading to zinc uptake into cells. Thus, the G280R mutation may cause electrostatic and steric interference, which may cause transporter protein destabilization (11). The G280R mutation had multiple deleterious effects including enhanced protein degradation, loss of vesicular localization, as well as the likely loss of zinc binding and consequently a markedly impaired zinc transport (Table 2). Substitutions of this residue to various amino acids demonstrated the functional importance of a small amino acid residue at this site. These findings are consistent with the severe phenotype that the G280R mother harbored as the zinc levels in her breast milk were very low (10 μg/dl at 4 months postpartum; normal range 80 ± 30 μg/dl) (11). Surprisingly, as revealed by two independent and complementary assays including BiFC and zinc toxicity, dimers of the mutant G280R together with WT-ZnT2 retained some vesicular localization and Zinquin accumulation function of the WT protein, thus demonstrating that the G280R did not exert a dominant-negative effect over the WT ZnT2.

In contrast to G280R, the T312M mutant displayed a minor impact on subcellular localization of WT-mutant ZnT2 dimers as well as on dimer formation. However, from our multiple analyses we can conclude that threonine 312 is an important component of the zinc permeation pathway, and substitution of this residue by a small or charged amino acid abolished zinc transport function. This T312M mutant was found to have the least deleterious effect on WT-ZnT2 among the 3 TNZD mutations studied here. This may also be related to the older age of TNZD onset in the infant of the mother carrying this T312M mutation (11).

Finally, E355Q is the mutant that presumably had the most deleterious effect on zinc coordination; moreover, our subcellular localization findings reveal that this mutation significantly altered the subcellular localization of ZnT2 dimers. These results suggest that zinc coordination at this residue, which is equivalent to site C in the bacterial YiiP transporter, has a major impact on protein stability. As such, substitution of this residue negatively affected not only zinc transport but also the structure and subcellular localization of ZnT2. Site C in YiiP was previously suggested to be critical for maintaining the stability of the protein (28). In summary, these three TNZD mutations markedly impaired the zinc transport function of ZnT2 in a multi-factorial manner as depicted in summarizing Table 2.

Using the BiFC assay we were able to follow the WT-mutant ZnT2 dimers and thereby determined the impact that specific heterozygous ZnT2 mutations had on the WT ZnT2. If the expression levels of the mutant and WT alleles are comparable in the breastfeeding mother, one expects to obtain 50% of the expressed protein in the homodimeric form composed of mutant-WT dimers, in addition to 25% of WT dimers as well as 25% of mutant-mutant dimers. As revealed by our flow cytometric analysis, the mutant-WT dimers are significantly more active in zinc transport than the mutant-mutant dimers, albeit remain less active in zinc accumulation when compared with WT homodimers. These results suggest that the residual activity of mutant-WT dimers is not sufficient to provide adequate zinc secretion into the breast milk. As we and others previously showed (16, 29), the refolding of the BiFC constructs into a fully fluorescent YFP protein is an irreversible process. Hence, the BiFC assay amplifies the percentage of the tagged BiFC dimers that are detected and thereby one can easily follow the localization and function of these various pairs. For example, mutant-WT pairs, which were tagged with BiFC, were preserved at the dimer state, and therefore our measurements mainly detected the function of these pairs. In contrast, in the zinc toxicity assay, the expression of WT-ZnT2 together with the mutant ZnT2, significantly compensated for the mutant ZnT2 function; indeed, cells were readily capable of handling almost the same zinc concentration of WT-ZnT2 expressing cells. These results indicate that G280R, T312M, and E355Q mutations did not significantly alter the function of the WT ZnT2 upon co-expression, hence raising the question of why mothers harboring a heterozygous *ZnT2* mutation produced breast milk that is very low in zinc and their infants presented with a severe TNZD phenotype. Excluding one case of compound *ZnT2* mutations (7), it is noteworthy that all reported cases of TNZD were heterozygous mutations. Although we have previously shown that the G87R mutation exerted a dominant-negative effect over the WT-ZnT2 (8, 17), the vast majority of other heterozygous inactivating ZnT2 mutations did not appear to exert a dominant-negative effect on the WT allele. Hence, although the inheritance pattern of TNZD has not yet been established, it appears to be dominant even in the heterozygote state. As a gradually increasing number of TNZD cases associated with heterozygous mutations in *ZnT2* was recently reported, one can suggest that the unaffected WT *ZnT2* allele in TNZD cases is certainly not sufficient to provide the necessary high levels of zinc in breast milk, which are strictly required for proper growth and development of the infant. Excluding cases of dominant-negative, such as the G87R mutation, the above results suggest a haploinsufficiency state for the unaffected WT *ZnT2* allele in TNZD pathology. Furthermore, the single case of premature stop codon (663delC), which was dominantly inherited (9), lends further support for haploinsufficiency, suggesting that one active copy of ZnT2 is not sufficient for adequate zinc secretion into breast milk. This latter mutation also strengthens the importance of the C terminus of ZnT2 in zinc transport, as upon deletion of this region, zinc levels in breast milk are clearly insufficient for the infant (9).

In fact, there is ample evidence that haploinsufficiency in heterozygous mutated transporter genes occurs in various diseases: (*a*) maternal riboflavin deficiency, resulting in transient neonatal-onset glutaric aciduria Type 2, is caused by a microdeletion in a single allele of the riboflavin transporter gene *GPR172B* (30). The authors postulated that haploinsufficiency of this riboflavin transporter causes riboflavin deficiency, and when coupled with nutritional riboflavin deficiency in pregnancy, could result in the transient riboflavin-responsive disease observed in the newborn infant. (*b*) Darier's disease, a skin disease characterized by dark crusty patches on the skin (dyskeratosis folicularis), is inherited in an autosomal dominant manner caused by heterozygous inactivating mutations in the *ATP2A2* gene (31). The latter encodes for the SERCA Ca^{2+}-ATPase, which serves as an ATP-driven intracellular Ca^{2+} pump located in the ER, hence actively concentrating Ca^{2+} into the ER lumen. In a recent study a novel heterozygous splice site mutation in the *ATP2A2* gene was identified, hence suggesting that despite heterozygous loss of function mutations in *ATP2A2*, the dominant inheritance in Darier's disease is due to haploinsufficiency (32). (*c*) Two genes that have been implicated as conferring susceptibility to autism spectrum disorder are phosphatase and tensin homolog (*PTEN*) and serotonin transporter (*SLC6A4*) (33). Recent studies in mice have concluded that haploinsufficiency occurs for mutant *PTEN* and serotonin transporter, which cooperatively influence brain size and social behavior. This is due to heterozygous mutations in both *PTEN* and serotonin transporter (33). As discussed above, it is likely that, in mammary epithelial cells, the expression of one WT *ZnT2* allele is not sufficient for the secretion of adequate zinc levels into breast milk. It was previously shown for the *BRACA1* gene that a heterozygous mutation is sufficient to largely increase the risk for cancer development in specific epithelial tissues like breast and ovary (34) with description of a unique mechanism, which contributes to tissue-specific cancer development. This may suggest that there is a specific mechanism that causes haploinsufficiency of *ZnT2* in mammary gland epithelial cells, as based on the current knowledge, *ZnT2* mutations are not known to affect other tissues and organs and did not induce other related symptoms in women carrying these mutations. However, post-translational modifications at the C terminus of ZnT2 were recently shown to be responsible for an altered subcellular localization of ZnT2 from early endosomes to lysosomes upon weaning (35). It will be interesting to investigate the effect of these different ZnT2 mutations presented in

the present study, all of which localized to the C terminus of ZnT2, on its localization during the weaning period.

In summary, our current findings regarding the mode of inheritance of TNZD suggest an autosomal dominant inheritance, although further studies with additional TNZD cases are required to establish this putative dominant autosomal inheritance. Based on a recent report, we have noticed that the case numbers of TNZD in Japanese women were significantly increasing in the past decade (11). These findings indicate that the number of TNZD cases may be higher than initially predicted, and may further increase with the encouragement of exclusive breast feeding, which is one of the main goals of the World Health Organization (WHO). In fact, to date only 38% of infants are exclusively breastfed globally, the WHO claims to increase exclusive breastfeeding to at least 50% of mothers until 6 months of age, by the year 2025. Further studies regarding new *ZnT2* mutations that cause TNZD in populations of distinct ethnicities are crucial for preventing morbidity of TNZD using proper genetic screening.

Author Contributions—Y. G. A. and T. K. conceived the study. Y. G. A. and Y. G. wrote the paper. Y. G. designed, performed, and analyzed the experiments shown in Figs. 1–4. N. I. and T. K. designed, performed, and analyzed the experiments shown in Figs. 5, 7, and 8 as well as Tables 3 and 5. F. G. designed, performed, and analyzed the experiments shown in Fig. 6 and Table 4. B. B. constructed the BiFC-mutated plasmids and provided technical assistance in these experiments.

References

1. Prasad, A. S. (2003) Zinc deficiency. *BMJ* **326,** 409–410
2. Huang, L., and Tepaamorndech, S. (2013) The SLC30 family of zinc transporters: a review of current understanding of their biological and pathophysiological roles. *Mol. Aspects Med.* **34,** 548–560
3. McCormick, N. H., Hennigar, S. R., Kiselyov, K., and Kelleher, S. L. (2014) The biology of zinc transport in mammary epithelial cells: implications for mammary gland development, lactation, and involution. *J. Mammary Gland Biol. Neoplasia* **19,** 59–71
4. Kambe, T. (2011) An overview of a wide range of functions of ZnT and Zip zinc transporters in the secretory pathway. *Biosci. Biotechnol. Biochem.* **75,** 1036–1043
5. Lessen, R., and Kavanagh, K. (2015) Position of the academy of nutrition and dietetics: promoting and supporting breastfeeding. *J. Acad. Nutr. Diet.* **115,** 444–449
6. Chowanadisai, W., Lönnerdal, B., and Kelleher, S. L. (2006) Identification of a mutation in SLC30A2 (ZnT-2) in women with low milk zinc concentration that results in transient neonatal zinc deficiency. *J. Biol. Chem.* **281,** 39699–39707
7. Itsumura, N., Inamo, Y., Okazaki, F., Teranishi, F., Narita, H., Kambe, T., and Kodama, H. (2013) Compound heterozygous mutations in SLC30A2/ZnT2 results in low milk zinc concentrations: a novel mechanism for zinc deficiency in a breast-fed infant. *PLoS ONE* **8,** e64045
8. Lasry, I., Seo, Y. A., Ityel, H., Shalva, N., Pode-Shakked, B., Glaser, F., Berman, B., Berezovsky, I., Goncearenco, A., Klar, A., Levy, J., Anikster, Y., Kelleher, S. L., and Assaraf, Y. G. (2012) A dominant negative heterozygous G87R mutation in the zinc transporter, ZnT-2 (SLC30A2), results in transient neonatal zinc deficiency. *J. Biol. Chem.* **287,** 29348–29361
9. Lova Navarro, M., Vera Casaño, A., Benito López, C., Fernández Ballesteros, M. D., Godoy Díaz, D. J., Crespo Erchiga, A., and Romero Brufau, S. (2014) Transient neonatal zinc deficiency due to a new autosomal dominant mutation in gene SLC30A2 (ZnT-2). *Pediatr. Dermatol.* **31,** 251–252
10. Miletta, M. C., Bieri, A., Kernland, K., Schöni, M. H., Petkovic, V., Flück, C. E., Eblé, A., and Mullis, P. E. (2013) Transient neonatal zinc deficiency caused by a heterozygous G87R mutation in the zinc transporter ZnT-2 (SLC30A2) gene in the mother highlighting the importance of Zn^{2+} for normal growth and development. *Int. J. Endocrinol.* **2013,** 259189
11. Itsumura, N., Kibihara, Y., Fukue, K., Miyata, A., Fukushima, K., Tamagawa-Mineoka, R., Katoh, N., Nishito, Y., Ishida, R., Narita, H., Kodama, H., and Kambe, T. (2016) Novel mutations in SLC30A2 involved in the pathogenesis of transient neonatal zinc deficiency. *Pediatr. Res.*, in press
12. Kambe, T., Tsuji, T., Hashimoto, A., and Itsumura, N. (2015) The physiological, biochemical, and molecular roles of zinc transporters in zinc homeostasis and metabolism. *Physiol. Rev.* **95,** 749–784
13. Kasana, S., Din, J., and Maret, W. (2015) Genetic causes and gene-nutrient interactions in mammalian zinc deficiencies: acrodermatitis enteropathica and transient neonatal zinc deficiency as examples. *J. Trace Elem. Med. Biol.* **29,** 47–62
14. Coromilas, A., Brandling-Bennett, H. A., Morel, K. D., and Chung, W. K. (2011) Novel SLC39A4 mutation in acrodermatitis enteropathica. *Pediatr. Dermatol.* **28,** 697–700
15. Alam, S., Hennigar, S. R., Gallagher, C., Soybel, D. I., and Kelleher, S. L. (2015) Exome sequencing of SLC30A2 identifies novel loss- and gain-of-function variants associated with breast cell dysfunction. *J. Mammary Gland Biol. Neoplasia* **20,** 159–172
16. Golan, Y., Berman, B., and Assaraf, Y. G. (2015) Heterodimerization, altered subcellular localization and function of multiple zinc transporters in viable cells using bimolecular fluorescence complementation. *J. Biol. Chem.* **290,** 9050–9063
17. Lasry, I., Golan, Y., Berman, B., Amram, N., Glaser, F., and Assaraf, Y. G. (2014) *In situ* dimerization of multiple wild type and mutant zinc transporters in live cells using bimolecular fluorescence complementation. *J. Biol. Chem.* **289,** 7275–7292
18. Fujimoto, S., Itsumura, N., Tsuji, T., Anan, Y., Tsuji, N., Ogra, Y., Kimura, T., Miyamae, Y., Masuda, S., Nagao, M., and Kambe, T. (2013) Cooperative functions of ZnT1, metallothionein and ZnT4 in the cytoplasm are required for full activation of TNAP in the early secretory pathway. *PLoS ONE* **8,** e77445
19. Sharma, M., Singh, A., Shankar, A., Pandey, A., Baranwal, V., Kapoor, S., Tyagi, A. K., and Pandey, G. K. (2014) Comprehensive expression analysis of rice Armadillo gene family during abiotic stress and development. *DNA Res.* **21,** 267–283
20. Webb, B., and Sali, A. (2014) Comparative protein structure modeling using MODELLER. *Curr. Protoc. Bioinformatics* **47,** 5.6.1–5.6.32
21. Pettersen, E. F., Goddard, T. D., Huang, C. C., Couch, G. S., Greenblatt, D. M., Meng, E. C., and Ferrin, T. E. (2004) UCSF chimera: a visualization system for exploratory research and analysis. *J. Comput. Chem.* **25,** 1605–1612
22. Meng, E. C., Pettersen, E. F., Couch, G. S., Huang, C. C., and Ferrin, T. E. (2006) Tools for integrated sequence-structure analysis with UCSF Chimera. *BMC Bioinformatics* **7,** 339
23. Schymkowitz, J., Borg, J., Stricher, F., Nys, R., Rousseau, F., and Serrano, L. (2005) The FoldX web server: an online force field. *Nucleic Acids Res.* **33,** W382–388
24. Pires, D. E., Ascher, D. B., and Blundell, T. L. (2014) DUET: a server for predicting effects of mutations on protein stability using an integrated computational approach. *Nucleic Acids Res.* **42,** W314–319
25. Lu, M., Chai, J., and Fu, D. (2009) Structural basis for autoregulation of the zinc transporter YiiP. *Nat. Struct. Mol. Biol.* **16,** 1063–1067
26. Lee, S., Hennigar, S. R., Alam, S., Nishida, K., and Kelleher, S. L. (2015) Essential role for ZnT2-mediated zinc transport in mammary gland development and function during lactation. *J. Biol. Chem.* **290,** 13064–13078
27. Murthy, S. C., Udagani, M. M., Badakali, A. V., and Yelameli, B. C. (2010) Symptomatic zinc deficiency in a full-term breast-fed infant. *Dermatol. Online J.* **16,** 3
28. Coudray, N., Valvo, S., Hu, M., Lasala, R., Kim, C., Vink, M., Zhou, M., Provasi, D., Filizola, M., Tao, J., Fang, J., Penczek, P. A., Ubarretxena-Belandia, I., and Stokes, D. L. (2013) Inward-facing conformation of the

zinc transporter YiiP revealed by cryoelectron microscopy. *Proc. Natl. Acad. Sci. U.S.A.* **110,** 2140–2145
29. Kerppola, T. K. (2009) Visualization of molecular interactions using bimolecular fluorescence complementation analysis: characteristics of protein fragment complementation. *Chem. Soc. Rev.* **38,** 2876–2886
30. Ho, G., Yonezawa, A., Masuda, S., Inui, K., Sim, K. G., Carpenter, K., Olsen, R. K., Mitchell, J. J., Rhead, W. J., Peters, G., and Christodoulou, J. (2011) Maternal riboflavin deficiency, resulting in transient neonatal-onset glutaric aciduria Type 2, is caused by a microdeletion in the riboflavin transporter gene GPR172B. *Hum. Mutat.* **32,** E1976–1984
31. Savignac, M., Edir, A., Simon, M., and Hovnanian, A. (2011) Darier disease: a disease model of impaired calcium homeostasis in the skin. *Biochim. Biophys. Acta* **1813,** 1111–1117
32. Huo, J., Liu, Y., Ma, J., and Xiao, S. (2010) A novel splice-site mutation of *ATP2A2* gene in a Chinese family with Darier disease. *Arch. Dermatol. Res.* **302,** 769–772
33. Page, D. T., Kuti, O. J., Prestia, C., and Sur, M. (2009) Haploinsufficiency for Pten and Serotonin transporter cooperatively influences brain size and social behavior. *Proc. Natl. Acad. Sci. U.S.A.* **106,** 1989–1994
34. Sedic, M., Skibinski, A., Brown, N., Gallardo, M., Mulligan, P., Martinez, P., Keller, P. J., Glover, E., Richardson, A. L., Cowan, J., Toland, A. E., Ravichandran, K., Riethman, H., Naber, S. P., Näär, A. M., Blasco, M. A., Hinds, P. W., and Kuperwasser, C. (2015) Haploinsufficiency for BRCA1 leads to cell-type-specific genomic instability and premature senescence. *Nat. Commun.* **6,** 7505
35. Hennigar, S. R., and Kelleher, S. L. (2015) TNFα post-translationally targets ZnT2 to accumulate zinc in lysosomes. *J. Cell. Physiol.* **230,** 2345–2350

Molecular Basis of Transient Neonatal Zinc Deficiency: NOVEL ZnT2 MUTATIONS DISRUPTING ZINC BINDING AND PERMEATION

Yarden Golan, Naoya Itsumura, Fabian Glaser, Bluma Berman, Taiho Kambe and Yehuda G. Assaraf

J. Biol. Chem. 2016, 291:13546-13559.
doi: 10.1074/jbc.M116.732693 originally published online May 2, 2016
